**Analysis of the configurations of a crystal surface. Pyrope (Mg2Al2Si3O12) as a case of study**

MASSARO F. R., BRUNO M., NESTOLA F.
Analysis of the configurations of a crystal surface. Pyrope (Mg2Al2Si3O12) as a case of study
CRYSTAL GROWTH & DESIGN (2014) 14
DOI: 10.1021/cg500065s

# Analysis of the configurations of a crystal surface. Pyrope ($Mg_3Al_2Si_3O_{12}$) as a case of study.

*Massaro F.R.,[1] Bruno M.,[2] Nestola F.[1]*

[1] Dipartimento di Geoscienze, Università degli Studi di Padova, Via Gradenigo 6, I-35131, Padova (Italy).

[2] Dipartimento di Scienze della Terra, Università degli Studi di Torino, Via Valperga Caluso 35, I-10125, Torino (Italy).

** corresponding author : francescoroberto.massaro@unipd.it*

**Abstract:**

This paper presents a work methodology to determine all the possible surface configurations of a *hkl* crystal face. As a case of study, we have applied our strategy to individuate the surface configurations of the {100}, {110} and {112} forms of pyrope ($Mg_3Al_2Si_3O_{12}$). In order to identify the most stable surface termination, we have performed an accurate *ab initio* study of the surface structures and energies at 0 K of the pyrope {100} configurations, by using the hybrid Hartree-Fock/Density Functional B3LYP Hamiltonian and a localized all-electron Gaussian-type basis set. Even if we are mainly interested in obtaining informations about the habit and genesis of natural garnets included in diamond (and pyrope is the main component of garnets trapped in diamonds), our results could be extremely useful to any researcher involved in the study of the surfaces of whatever crystalline phase.

## 1. Introduction

Garnet, particularly pyrope ($Mg_3Al_2Si_3O_{12}$; space group $Ia\bar{3}d$; $a_0$ =11.4545 Å; $\alpha = \beta = \gamma = 90°$),[1] is a common high-pressure phase; together with other phases such as zircon ($ZrSiO_4$), diamond (C), topaz ($Al_2SiO_4(OH)_2$) and coesite ($SiO_2$), it is typical of the ultrahigh-pressure rocks like eclogites. Nevertheless, garnets are rather common as ultramafic igneous rock-forming minerals, as in the case of peridotites or kimberlites and among the most abundant minerals found as inclusions in diamonds.

From the mineralogical point of view, garnets are nesosilicates with a general formula $M_3N_2[XO_4]_3$.[2] In natural garnets: X stands for the tetravalent cation $Si^{4+}$; M (large divalent cation with coordination number equal to eight) is $Ca^{2+}$ in the ugrandite (uvarovite + grossular + andradite), $Mg^{2+}$ in pyrope, $Fe^{2+}$ in almandine and $Mn^{2+}$ in spessartine; N (small trivalent cation with coordination number equal to six) is $Al^{3+}$ in the pyralspite series (pyrope + almandine + spessartine), $Fe^{3+}$ in andradite and $Cr^{3+}$ in uvarovite. The crystal structure is a three-dimensional network in which the isolated X-tetrahedra share vertices with the N-octahedra, and large distorted cubic sites (dodecahedra) are occupied by the large M cation.

Our interest for pyropic garnets is justified by the fact that they are typical diamond inclusions (DIs) in peridotitic rocks belonging to the harzburgitic variety (here the garnets could show up to 80-85% of pyrope component), along with orthopyroxene, diopsidic clinopyroxene, forsteritic olivine, magnesium chromite and iron–nickel sulfides. However, the pyrope component is extremely important also for garnets found as inclusions in eclogitic diamonds (where the pyrope fraction could easily reach 40%).[3] Studying DIs plays a key role in understanding and interpreting the geodynamics, geophysics, petrology, geochemistry and mineralogy of Earth's mantle.[4] On the base of their origin, DIs are divided into three categories: *proto-*, *syn-* and *epigenetic*.[5] DIs are classified as protogenetic when they crystallize before the encapsulation by the host diamond, whereas they are considered syngenetic when the inclusion and its host diamond form at the same time originating from the same genetic process. Both categories play a crucial role for understanding the diamond formation processes; on the contrary, epigenetic phases, i.e.: secondary minerals, are usually connected to crustal processes and atypical with respect to the primary minerals in mantle xenoliths.

Discerning between syngenesis and protogenesis is as critical as controversial, as demonstrated by Taylor *et al.*[6] The most common feature considered to deduce syngenesis is the morphological control of the DI shape by the host diamond morphology.[5,7-9] Sobolev *et al.*[10] stated that the octahedral morphology, exclusively observed in the pyropic DIs, was imposed by the diamond as a consequence of the growth of garnet in etched pits on diamond {111} growth surfaces. Other authors[11] thought that the inclusion morphology developed as a result of a mutual growth during which the greater 'form energy' of diamond would have imposed its morphology upon the inclusion. For what concerns the few clues of protogenesis, Meyer[5] wrote that the inclusions that formed before their encapsulation in diamonds typically should show either irregular morphologies or euhedral morphologies that are closely related to the crystal structure of the mineral. Another substantial contribution to the syngenesis/protogenesis debate comes from the observation that some DIs occur in a specific orientation with respect to diamond; this can be

believed as a proof of somewhat epitaxial relationship between DI and diamond, and hence of syngenesis.[5,7,9,11-17]

A comprehensive knowledge of garnet surface energy and morphology at the atomic level is of extreme importance to understand the true nature of these and, more generally, all those processes involving the garnet interface (i.e.: epitaxial relationships with others phases, adsorption of atoms and molecules on the crystal faces, mechanisms of reactions involving the surfaces). Indeed, in order to simulate and understand the chemical processes occurring on a crystal surface requires the knowledge of its most probable surface termination (or structural configuration), that is the surface termination having the lowest surface energy. Unfortunately, as we will show in this paper, the determination of the most probable configuration for chemically and structurally complex phases like pyrope, is a very difficult task. Then, it is not surprising that, at the best of our knowledge, no calculations whose purpose is to evaluate the energy or the detailed configurations of garnet surfaces have ever been made. Instead, only a few theoretical studies on the main surfaces of garnets have been performed until now. In particular, Boutz and Woensdregt[18] predicted the growth morphology of garnets by means of the attachment energies computed by means of an electrostatic point charge model basing on the Periodic Bound Chain (PBC) analysis carried out by Bennema *et al.*.[19] Dealing with their level of detail in studying the surfaces terminations, these authors wrote, referring to all the surfaces with no distinction: <<*…Now it is possible to define an F face with statistically disordered surface of boundary ions, i.e.: all the boundary ion sites have an occupancy of fifty percent. On the other hand energetically most stable surface is that with the ordered surface configuration, i.e.: only half of the ion site are fully occupied…*>>, without performing a detailed analysis of the possible surface configurations by adopting the criteria that we show in the present paper.

In order to identify the main surfaces of pyrope to study in this work, we took inspiration by previous papers where morphological observations of natural and synthetic garnet crystals are reported.[20-23] According to these works, the garnet crystals are characterized by a few recurrent crystallographic forms, namely the {110} and {112}. Special attention was given to the work of Bennema *et al.*:[19] their PBC analysis on the garnet structure revealed that the {112}, {110}, {100}, {210}, {321}, and {322} forms (the order is a consequence of the morphological importance attributed by the authors) were classified as *F* (flat) according to the Hartman-Perdok theory,[24-26] so they have the best chances to characterize the final morphology of the crystal. Among all the forms, the {100} draws a special interest since it is, along with the {111}, a crystallographic form occurring only in the DIs and never in the not-encapsulated natural garnets, thus potentially able to give specific information about the syngenesis/protogenesis debate. For all these reasons, we

performed a detailed configurational analysis of the (100), (110) and (112) surfaces and *ab initio* quantum-mechanical calculations about all the possible (100) configurations adopting a hybrid Hartree-Fock (HF)-DFT approach, which has never been applied before to the study of pyrope surfaces. In detail, the chosen functional is B3LYP,[27-29] which has already proved great accuracy in describing the surfaces of diamond and forsterite ($Mg_2SiO_4$).[30,31]

Finally, the aim of the present paper is not to compute the theoretical equilibrium or growth shapes of garnet, but rather to define a way of correctly treating in detail all the surfaces when working with whatever crystal, taking as examples the {100}, {110} and {112} forms of pyrope.

The paper is structured as follows: (i) illustration of the computational techniques and parameters used in the *ab initio* calculations; (ii) description of the surface configurations for the {100}, {110} and {112} forms of pyrope crystals; (iii) analysis about the surface energies and the variations of bond distances and angles for all the possible {100} surface configurations; (iv) main conclusions.

## 2. Computational details

The *ab initio* CRYSTAL09 code[32,33] was employed, which implements the Hartree-Fock and Kohn-Sham self-consistent field (SCF) method for the study of periodic systems.[34] The crystal surfaces were simulated by using the 2D periodic slab model, consisting of a film formed by a set of atomic layers parallel to the *hkl* crystalline plane of interest.[35]

All the calculations were performed at the DFT (Density Functional Theory) level. In the Density Functional approach, the B3LYP Hamiltonian was adopted,[27-29] which contains a hybrid Hartree-Fock/Density-Functional exchange term and already shown to provide accurate results for structural and dynamical properties of garnet end members.[36]

In CRYSTAL the multi-electronic wave-function is constructed as an anti-symmetrized product (Slater determinant) of mono-electronic crystalline orbitals (COs) which are linear combinations of local functions (i.e.: atomic orbitals, AOs) centered on each atom of the crystal. In turn, AOs are linear combinations of Gaussian-type functions (GTF, the product of a Gaussian times a real solid spherical harmonic to give *s*-, *p*- and *d*-type AOs). In this study, aluminum, silicon, oxygen, and magnesium were described by (8*s*)-(511*sp*)-(1*d*), (8*s*)−(6311*sp*)−(1*d*), (8*s*)−(411*sp*)−(1*d*), and (8*s*)−(511*sp*)−(1*d*) contractions, respectively. The exponents (in $bohr^{-2}$ units) of the most diffuse *sp* shells are 0.59 and 0.35 (Al), 0.32 and 0.13 (Si), 0.59 and 0.25 (O), and 0.68 and 0.22 (Mg); the exponents of the single Gaussian *d* shell are 0.51 (Al), 0.6 (Si), 0.5 (O), and 0.5 (Mg).[37-38]

The thresholds controlling the accuracy in the evaluation of Coulomb and exchange integrals (ITOL1, ITOL2, ITOL3, ITOL4 and ITOL5, see Dovesi *et al.*[33]) were set to $10^{-8}$ (ITOL1 to ITOL4) and $10^{-16}$ (ITOL5). The threshold on the SCF energy was set to $10^{-8}$ Hartree.

In the adopted package the DFT exchange and correlation contributions are evaluated by numerically integrating functions of the electron density and of its gradient over the cell volume. The choice of the integration grid is based on an atomic partition method, originally developed by Becke.[39] In the present study, a *pruned* (75, 974) *p* grid was adopted (XLGRID in the code[33]), which ensured a satisfactory accuracy in the numerically integrated electron charge density (the error is on the order of $1 \cdot 10^{-4}$ |e| on a total of 1120 |e| for all the considered surfaces).

The reciprocal space was sampled according to a Monkhorst-Pack mesh[40] with shrinking factor 4, corresponding to 10 **k** and 8 **k** points in the first irreducible Brillouin zone in the slabs e bulk, respectively.

Structures were optimized by using the analytical energy gradients with respect to atomic coordinates and lattice parameters within a quasi-Newton scheme, combined with the Broyden-Fletcher-Goldfarb-Shannon scheme for Hessian updating.[41-43] Convergence was checked on energy, gradient components and nuclear displacements. The threshold on energy between two subsequent optimization steps was set to $10^{-7}$ Hartree; the thresholds on the root-mean-square of the gradient components and of the nuclear displacements were set to $3.0 \cdot 10^{-4}$ Hartree bohr$^{-1}$ and $1.2 \cdot 10^{-3}$ bohr, respectively; those on the maximum components of the gradients and displacements were set to $4.5 \cdot 10^{-4}$ Hartree bohr$^{-1}$ and $1.8 \cdot 10^{-3}$ bohr, respectively.

The specific surface energy $\gamma$ (J/m$^2$) at T = 0K was calculated by using the following relation:[35]

$$\gamma = \lim_{n\to\infty} E_s(n) = \lim_{n\to\infty} \frac{E(n)_{slab} - nE_{bulk}}{2A} \quad (1)$$

where $E(n)$ is the energy of a $n$-layer slab; $E_{bulk}$ is the energy of the bulk; $A$ is the area of the primitive unit cell of the surface; the factor 2 in the denominator accounts for the upper and lower surfaces of the slab. $E_s(n)$ is thus the energy per unit area required for the formation of the surface from the bulk. As more layers are added in the calculation ($n \rightarrow \infty$), $E_s(n)$ will converge to the surface energy per unit area ($\gamma$).

The thicknesses of the slabs used to simulate the configurations *cut1* and *cut2* of the (100) face are ~13 Å (with 160 atoms) and ~15 Å (with 200 atoms), respectively (see the Supporting Information); all of these slabs are charge neutral and retain the centre of inversion, to ensure that

the dipole moment perpendicular to the slab is equal to zero. A satisfactory convergence on structure is not yet reached and, as a consequence, thicker slabs should be considered. Unfortunately, the system studied is extremely expensive from a computational point of view and our calculus resources are not adequate, then we are not able to verify the criterion of convergence concerning the structure. Nevertheless, the slab thicknesses considered in this work are sufficient to obtain reliable surface energy values, which allow us to evaluate the most probable surface configuration. Indeed, previous ab initio calculations performed with the same basis set, hybrid functional and computational parameters of this work on forsterite surfaces,[31] demonstrated that slab thickness of 14-15 Å are sufficient to reach convergence on surface energy values.

## 3. Configurational analysis of the pyrope surfaces

When a geometry optimization is performed, an initial crystal structure must be supplied to the program, i.e.: in our case as input in the CRYSTAL09 code. Then, the program will be able to find an optimized structure: if the initial structure is somewhat far away from the equilibrium one, it is highly likely that the resulting optimized structure does not correspond to the absolute minimum of the potential energy surface, but to a local (relative) one. This implies that to increase the probability to individuate the structure associated to the absolute minimum, several guess structures must be tested.

As concerns the study of the surfaces, the most stable slab structure must be sought among all the possible initial (then not optimized) surface configurations of the studied face (i.e.: all the possible slab terminations obtained by the cut of the bulk structure), which can be identified by performing a careful analysis of the bulk structure of the phase, as detailed below.

### 3.1. A strategy to determine the surface configurations

Chemically and structurally complex phases like garnet can show a huge number of initial surface configurations. To find them is a very difficult task that requires a careful analysis of the structure and symmetry of the surface. For such a reason, in this section, we attempt to define a *work methodology* to apply to the study of any crystalline surface. In particular, we are interested to the study of stoichiometric surfaces: neutral slabs made up by an integer number ($n$) of formula units, i.e.: $n\cdot(Mg_3Al_2Si_3O_{12})$. Not stoichiometric surfaces will not be taken into account in this work, as their study requires a very different approach with respect to that we adopted for the stoichiometric ones.

From an operative point of view, the procedure to adopt for the surface configurations analysis is the following:

a) Generation of the *slab*. It is obtained by cutting the bulk structure along the *hkl* plane defining the face to study, this implies the possibility to have a certain number of *cuts* placed at different levels of the bulk structure. As a general rule, the more complex the crystal structure and chemical composition, the larger the number of cuts.

b) Determination of the *surface configurations* from each cut, whose number is the consequence of the different ways to remove the atoms from the outermost layers of the slab for obtaining a stoichiometric one. For clarity of presentation, we will use the following notation: (i) the term *reconstruction* indicates the procedure of atoms removal to build a stoichiometric slab; (ii) atoms having the same z-coordinate (in this case according to the perpendicular to the plane of interest) in a not optimized slab, are considered to form a *layer*, and (iii) for each crystal face, a slice of variable thickness is defined (named *reconstruction slice*, RS), which is composed by the minimum number of outermost layers involved in the surface reconstruction. As we will see, the number of configurations is a function of the crystal face symmetry and of the removal percentage of each atomic type in the RS.

Below, the number and type of initial surface configurations of the {100}, {110} and {112} faces of pyrope are determined. Here, for what concerns the pyrope surface reconstruction, it is necessary to point out that:

(i) the slab were cut starting from the optimized bulk structure: $a_0$ = 11.5451 Å and $\alpha = \beta = \gamma$ = 90°;

(ii) the oxygen elimination is realized without affecting the bonds in the silica tetrahedra, the Si-O bond being the strongest in a silicate framework. This is the only constraint we impose to perform the reconstruction of the slabs for pyrope.

### 3.1.1. {100} form

Projecting along the <100>, we can imagine the garnet structure as a stacking of slices containing $SiO_4$ tetrahedra and $MgO_8$ dodecahedra, and slices built by the same polyhedra with the $AlO_6$ octahedra in addition.

The (100) face belongs to the layer group *P112/a*, thus the symmetry elements which have to be taken into account to perform a surface reconstruction are the two-fold axes perpendicular to the face. By analysing the (100) slab structure, two cuts (*cut1* and *cut2*) can be envisaged having a square surface cell (surface vectors belonging to the <100> directions equal to 11.5451 Å and $\gamma$ = 90°) with four equivalent two-fold axes.

As concerns *cut1*, the RS is formed by three layers forming two independent $SiO_4$ and two independent Mg alternating along the x and y axes, whose centres of mass coincide with the two-fold axes (left of Figure 1). For obtaining a stoichiometric slab, one $SiO_4$ and one Mg have to be deleted from each cell. As the two-fold axis coincide with the Si and Mg cations, four not equivalent surface configurations originate, in the following named *cut1a-d*. Interestingly, whatever $SiO_4$ and Mg are removed, the symmetry of the (100) face results to be preserved.

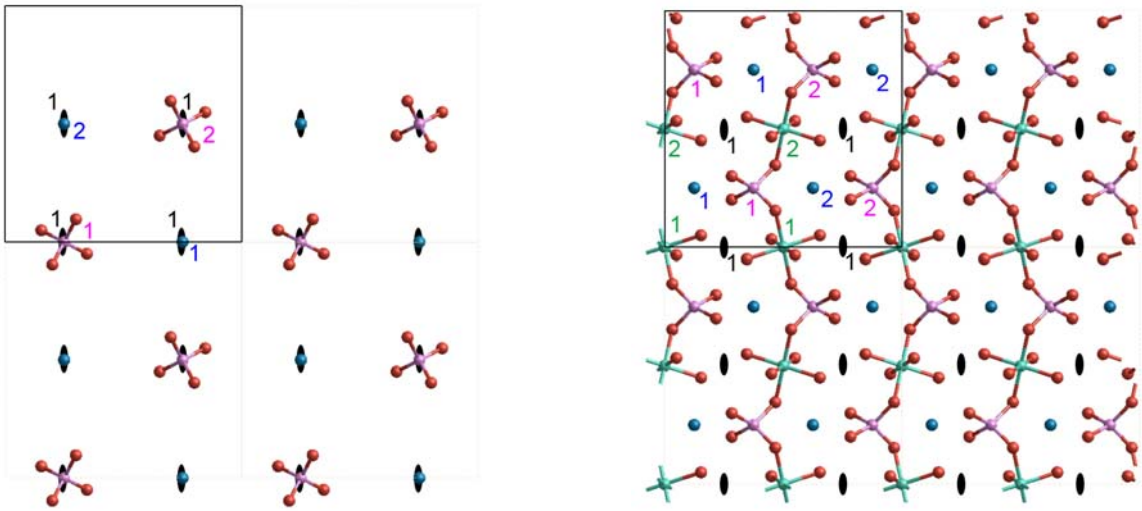

**Figure 1 –** The (100) reconstruction slice cells according to the *cut1* (left) and the *cut2* (right). The structure is viewed along the [100] direction. The colours stand: red for the O, pink for the Si, green for the Al, blue for the Mg ions and black for the two-fold axes. Numbers give information about the type of cations or two-fold axes.

The *cut2* has a higher atomic density with respect to the *cut1*. Indeed, the RS is composed by nine layers forming four $SiO_4$, four $AlO_6$ and four Mg (two of type 1 and two of type 2, see the right of Figure 1). The stoichiometric reconstruction implies the elimination of two $SiO_4$, two $AlO_6$, two Mg and the oxygens necessary not to leave unsaturated $SiO_4$ tetrahedra. Two cases can be envisaged:

(i) the symmetry of the (100) face is respected, that is the two-fold axis are preserved. Then, only eight independent configurations are detected, *cut2a-h*. The number of these configurations ($N_C$) is given by the relation:

$$N_C = \prod_i C_i \quad (1)$$

where $C_i$ ($i$ = Mg, Si, Al) = 2 is the number of ways in which is possible to remove two atoms of type $i$ every four by preserving the two-fold axis.

(ii) The symmetry of the (100) face is neglected. In this case the number of configurations is calculated with the equation:

$$N_C = \prod_{i=Si,Al} \frac{S_i!}{A_i!(S_i - A_i)!} \quad (2)$$

where $S_i$ is the number of crystallographic sites in which the number of atoms $A_i$ of type $i$ = Si, Al can be placed. Then, being $A_i = 2$ and $S_i = 4$ for both Si and Al, $N_C = 36$. The Mg does not enter into eq. (2) because it is taken as the reference sub-lattice with respect to which the others atoms (Si and Al) are arranged. Indeed, if only the layer of Mg cations in RS is considered, the removal of any two atoms always generates the same sub-lattice. The thirty-six configurations are a consequence of the different ways to arrange the Si and Al atoms with respect to the Mg sub-lattice.

In this work we are only interested to the study of the surface configurations respecting the symmetry of the face, as we previously demonstrated[44-48] that such surfaces are associated to lower surface energy values, thus they have a higher chance to exist at the equilibrium or in growth. Therefore, the most stable surface termination is to research into the twelve initial configurations *cut1a-d* and *cut2a-h*, those preserving the two-fold axis. In the following, the surface energy values and optimized structures of these twelve configurations obtained at *ab initio* level will be discussed.

### 3.1.2. {110} form

Projecting along the <110> or the <100>, we can imagine the garnet structure as a stacking of $d_{110}$ slices made by $SiO_4$ tetrahedra, $MgO_8$ dodecahedra and $AlO_6$ octahedra placed at different height.

As in the case of the (100) face, the (110) belongs to the layer group *P112/a*. From the analysis of the (110) slab structure, a cut (*cut1*) was only found with a rectangular 2D cell limited by <110> (=16.1991 Å) and <100> vectors and γ = 90°. The RS is formed by eighteen layers with four $SiO_4$, four Mg and eight $AlO_6$, with Si and Mg lying on a same layer (i.e.: same z coordinate) and Al placed at slightly lower z; the $AlO_6$ can be grouped according their equivalences in type 1 and 2. Moreover, the 2D cell includes eight two-fold axes of two types perpendicular to the plane as well (Figure 2). It is worth noting that such a cell is not the primitive one, but a supercell containing the minimum amount of atoms that allows to perform the reconstruction in order to obtain a stoichiometric slab.

In order to follow the stoichiometric rule, a 25% reconstruction is needed: it determines the loss of one cation every four in the Si-Mg layer and of two Al every eight. In every case the symmetry of the faces falls down (from *P112/a* to $P\bar{1}$), thus causing the loss of the possibility to study only the higher symmetry configurations. Matching the four possible configurations for the

Si-Mg level and the twenty-eight in the Al layer, one hundred and twelve (112) feasible configurations are obtained. This number is the consequence of the application of the relation (2), by inserting $A_{Si} = 1$, $A_{Al} = 2$, $S_{Si} = 4$ and $S_{Al} = 8$.

The high number of initial surface configurations prevents the possibility to evaluate their surface energies and structures by means of *ab initio* calculations. Therefore, for the (110) face the *ab initio* calculations were not performed in this work, we determined only its number of initial surface configurations.

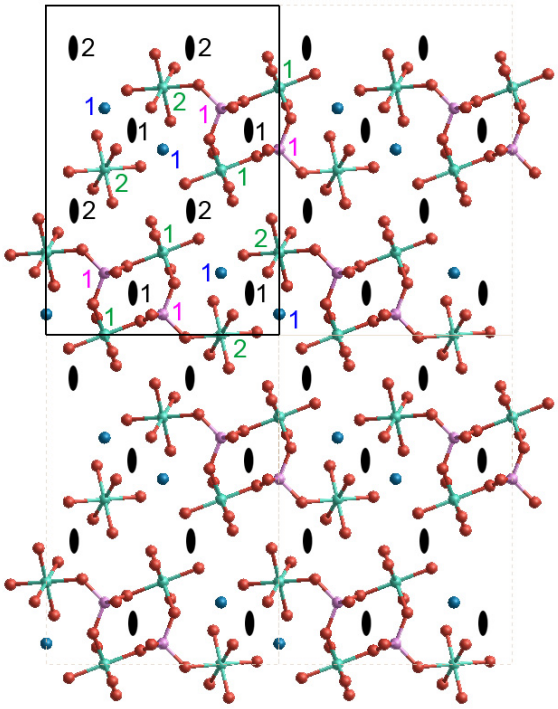

**Figure 2 -** The (110) reconstruction slice cell projected along the [110] direction.

### 3.1.3. {112} form

We can imagine the garnet structure as succession of two different types of slices containing $SiO_4$, $MgO_8$ and $AlO_6$ polyhedra, stacked along the <112> directions. In this case the surface belongs to the layer group $P\bar{1}$, then the only element of symmetry to preserve when a reconstruction is performed is the inversion center; its surface cell is limited by the <111> (=19.8398 Å) and <110> vectors with $\gamma = 90°$. Two cuts can be determined (Figure 3):

(i) the RS of *cut1* is built by seventeen layers and contains eight $AlO_6$ and eight Mg together with four $SiO_4$; while Al and Mg lie on the same layer, Si has a slightly higher z-coordinate;

(ii) the RS of *cut2* is formed by eighteen layers and includes eight $AlO_6$ and eight $SiO_4$; even in this case two cations (Al and Si) are on the same layer while one (Mg) has a slightly higher z-coordinate.

As concerns *cut1*, the stoichiometry of the slab is reached by removing one $SiO_4$ every four, two $AlO_6$ every eight and one Mg every eight. As in the case of the (110) face, we have one hundred and twelve (112) configurations deriving by relation (2) with $A_{Si} = 1$, $A_{Al} = 2$, $S_{Si} = 4$ and $S_{Al} = 8$.

The stoichiometry of the *cut2* is instead obtained by erasing two Mg every eight, two $AlO_6$ every eight and one $SiO_4$ every eight. This leads to two hundred and twenty-four (224) configurations for this cut ($A_{Si} = 1$, $A_{Al} = 2$, $S_{Si} = 8$ and $S_{Al} = 8$ in relation (2)).

As a consequence, we have three hundred and thirty-six (336) surface configurations for the (112) face.

As in the case of the (110) face, this high number initial surface configurations prevents the possibility to evaluate their surface energies and structures at *ab initio* level.

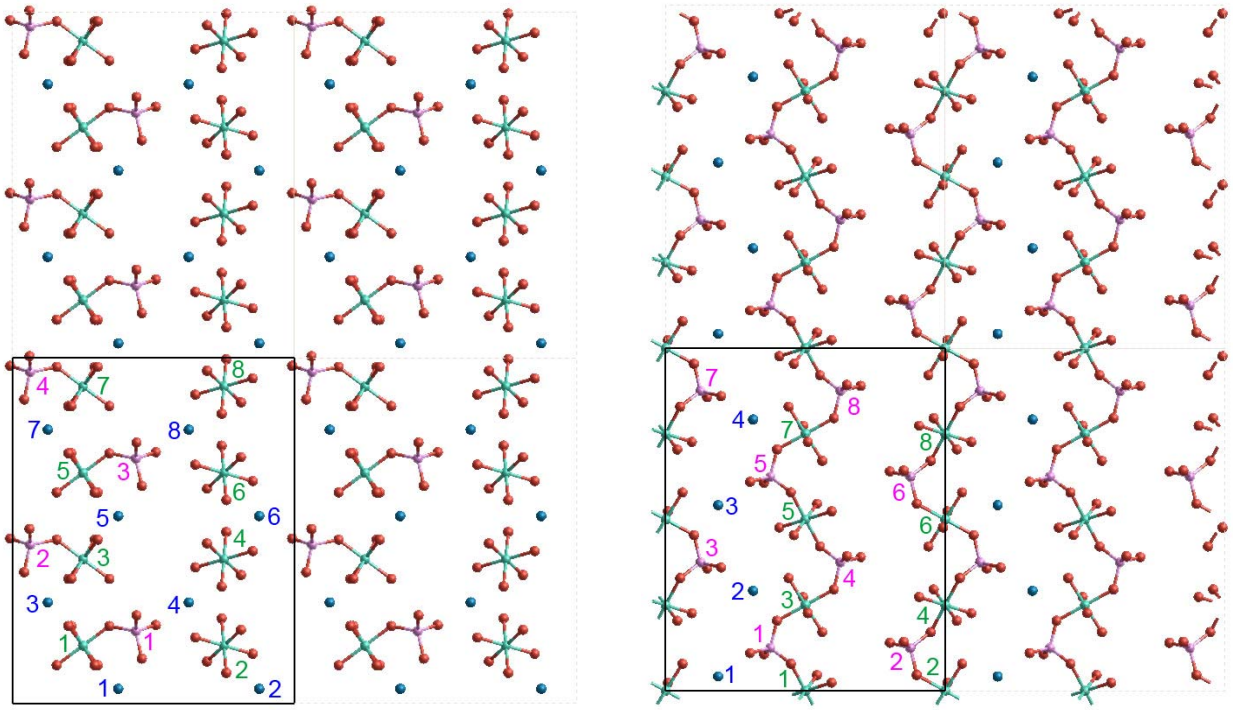

**Figure 3** - The (112) reconstruction slice cells according to the *cut1* (left) and the *cut2* (right). The structure is viewed along the [112] direction.

## 4. Results and discussion.

In this section, the energetic and structures of the optimized (100) surface configurations will be discussed. Table 1 lists the surface energies at 0K ($\gamma$) of the twelve possible initial configurations of the {100} crystallographic forms analyzed in this work. The configurations with the lowest surface energy result to be the *cut1d* and *cut2d*; they are showed in the relaxed and unrelaxed state in Figure 4, whereas the drawings of all the others unrelaxed and relaxed geometries are reported in the Supporting Information. Moreover, the CRYSTAL09 output files are freely available at http://mabruno.weebly.com/download.

The optimized geometry of the *cut1d* differs more from the bulk one respect to that of the *cut2d*, the $SiO_4$ tetrahedra being inclined to mainly distort so that the uppermost oxygens can lower to flatten down on the surface. There is a correspondence between this surface structural modification and the stability of the surface since this cut is associated to the lowest surface energy. The examination of the relaxed structures (see also the Supporting Information) let one deduce that the twelve cuts are sorted two by two if taking into account the geometrical affinities. This observation is confirmed by the surface energies data that are nearby (the little differences can be ascribed to the numerical error during energy minimization), if referred to surface cuts that are similar from a geometrical point of view. The couples of surfaces of a kind ordered by decreasing of stability are *cut1d* and *1a* (upper left of Figure 4 and Figure S1), *2d* and *2e* (down left of Figure 4 and Figure S7), *1b* and *1c* (Figures S2 and S3), *2b* and *2h* (Figures S5 and S10), *2a* and *2f* (Figures S4 and S8), *2c* and *2g* (Figures S6 and S9).

Some further considerations on these equalities can be done. In particular, it is interesting to point out that, after the optimization procedure, the twelve initial surface configurations have became six, among which we are able to distinguish: (i) the absolute minimum of the potential energy surface corresponding to the optimized structure of *cut1a* and *1d*; (ii) five local minima corresponding to the others optimized structures. As listed in Table 1, the percentage variation of the surface energy of the *i*-th configuration with respect to the most stable one (*cut1d*) results to be ~4-5%, ~12%, ~28-32%, ~45-49% and ~71% for *cut2d*(*2e*), *cut1b*(*1c*), *cut2b*(*2h*), *cut2a*(*2f*) and *cut2c*(*2g*), respectively. Interestingly, a very small difference (~4-5%) is observed between the lowest surface energy value of the *cut1* configurations (*1a* and *1d*) and the lowest one of the *cut2* configurations (*2d* and *2e*). This suggests that the probability to have a (100) surface with the *1a*(*1b*) or *2d*(*2e*) configuration is very similar.

**Table 1. Surface energies at 0K of all the possible configurations of {100} pyrope. We also report the $\Delta\gamma$ (%) = $[(\gamma_i - \gamma_{cut1d})/ \gamma_{cut1d}]\times100$ for the *i*-th configuration, to stress its variation with respect to the most stable one (*cut1d*).**

| *cut* | {100} surface energies | $\Delta\gamma$ | *cut* | {100} surface energies | $\Delta\gamma$ |
|---|---|---|---|---|---|

| | [J/m$^2$] | [%] | | [J/m$^2$] | [%] |
|---|---|---|---|---|---|
| *1a* | 1.720 | 0.5 | *2c* | 2.930 | 71.1 |
| *1b* | 1.911 | 11.6 | *2d* | 1.781 | 4.0 |
| *1c* | 1.910 | 11.6 | *2e* | 1.791 | 4.6 |
| *1d* | 1.712 | 0.0 | *2f* | 2.551 | 49.0 |
| *2a* | 2.491 | 45.5 | *2g* | 2.929 | 71.1 |
| *2b* | 2.265 | 32.3 | *2h* | 2.189 | 27.9 |

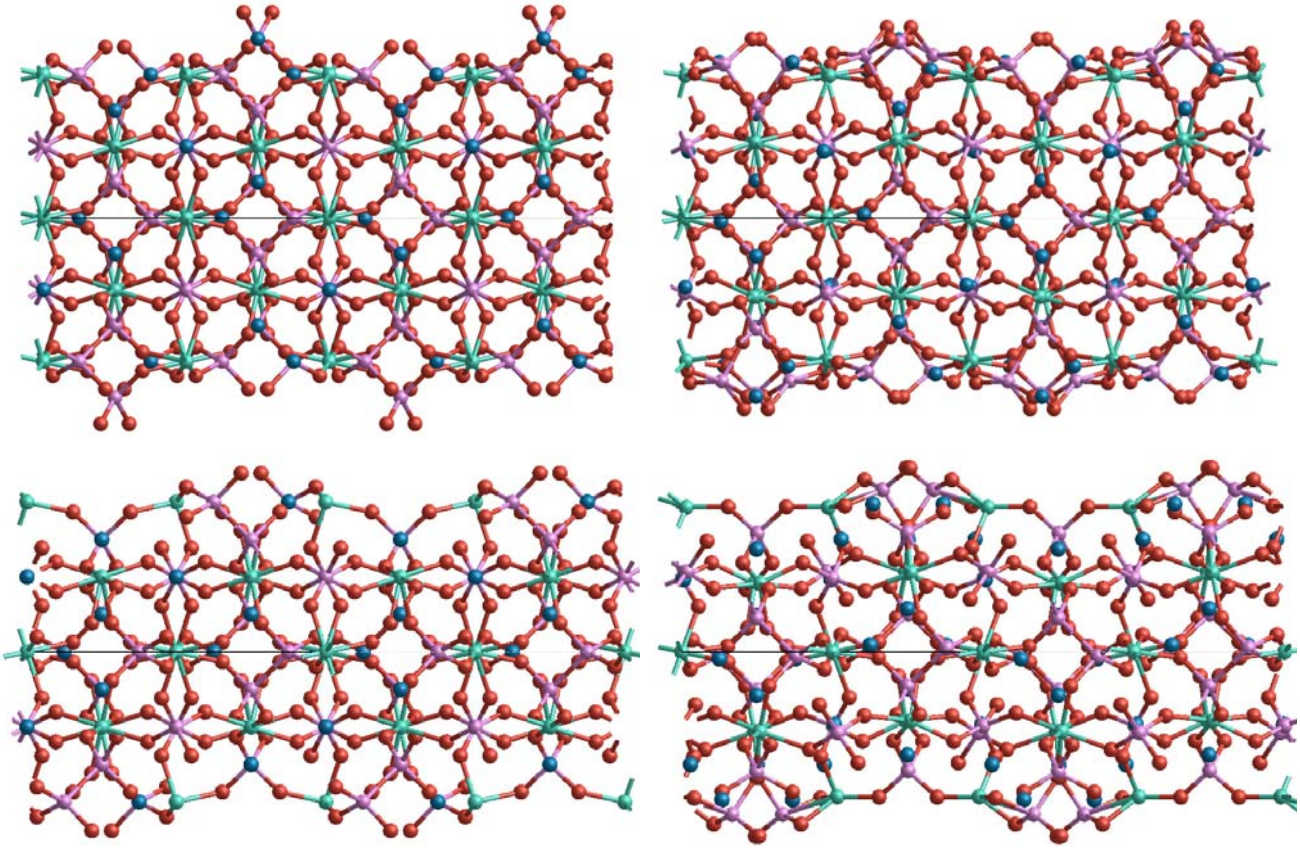

**Figure 4 -** The lowest energy {100} slab for the *cut1* (up) and the *cut2* (down), before (left) and after (right) the geometry optimization. The structure is projected along the equivalent <100> directions.

In the following part, some considerations about the modifications of the Cation-Oxygen bond lengths and of the Oxygen-Cation-Oxygen angles are discussed.

After the reconstruction and before the geometry optimization, the {100} surface cell in the *cut1* configurations preserves one $SiO_4$ tetrahedron and one Mg polyhedron deprived of four oxygens. The four Si-O distances per tetrahedron are identical in the bulk and equal two by two in

the surface, while the Mg-O bonds are eight and grouped four by four in the bulk, but only four, sorted two by two, in the surface cell. In the *cut2* configurations, every surface cell includes four different distances for each cationic species of the garnet structure. This is for, as already pointed in the previous paragraph, our reconstruction technique allows only to tetrahedra to preserve their own anions, while each uppermost aluminium looses two oxygens every six and each uppermost Mg preserve four oxygens every eight.

Table 2 reports the values for the Si-O, Al-O and Mg-O bond distances for the optimized bulk and the two cuts according to which it is possible to realize stoichiometric {100} surfaces. Two statistical indices are adopted to summarize the effect of atomic relaxation: the average Cation-O bond distance per polyhedron, <Cation-O> [Å], and the difference between the maximum and the minimum bond distance per polyhedron, Δ [Å].

The average values calculated for the Si-O, Al-O and Mg-O bulk distances are 1.6495, 1.9004 and 2.2841 Å, respectively. The highest Si-O and Al-O variations with respect to the bulk values (+0.92 and -6.49%, respectively) are observed in *cut2d*, while in the case of the Mg-O bonds (-15.19%) for the *cut1d*. The max Δ values are registered in the *cut2d* case: they are 0.1411, 0.1501 and 0.2864 Å for the Si-O, Al-O and Mg-O distances, respectively. From the evaluation of the Cation-O distances one can deduce that the Mg and Al surface cations, which lose their original coordination (i.e.: the bulk coordination), result to be more attracted by their first-neighbours oxygens. The same thing does not happen in the case of Si, for which a weak rise of the Si-O bond length is observed in the most energetically stable among the *cut2* configurations.

**Table 2. Optimized Si-O, Al-O and Mg-O bond distances [Å] of pyrope and of its (100) surface according to the two lowest energy terminations at 0 K, each for the two kinds of cut. Surface data are reported for the symmetry independent polyhedra included in the reconstruction slice. <Cation-O> [Å] is the average bond length per polyhedron; Δ [Å] is the difference between the maximum and minimum Cation-O distance values. The relative % difference of <Cation-O> and Δ with respect to the bulk, and the multiplicity m of the bulk bonds are reported.**

| bond | m | bulk | (100) | | bond | m | bulk | (100) | bond | m | bulk | (100) | |
|---|---|---|---|---|---|---|---|---|---|---|---|---|---|
| | | | *cut1* | *cut2* | | | | *cut2* | | | | *cut1* | *cut2* |
| Si-O | 4 | 1.6495 | 1.5981 | 1.5794 | Al-O | 6 | 1.9004 | 1.7029 | Mg-O | 4 | 2.2046 | 1.8876 | 1.9293 |
| | | | 1.5981 | 1.6435 | | | | 1.7737 | | 4 | 2.3636 | 1.8876 | 1.9409 |
| | | | 1.6962 | 1.7156 | | | | 1.8084 | | | | 2.0782 | 2.0512 |
| | | | 1.6962 | 1.7205 | | | | 1.8530 | | | | 2.0782 | 2.2157 |
| <Si–O> | | 1.6495 | 1.6472 | 1.6648 | <Al–O> | | 1.9004 | 1.7845 | <Mg–O> | | 2.2841 | 1.9829 | 2.0343 |
| | | | -0.14% | +0.92% | | | | -6.49% | | | | -15.19% | -12.28% |
| Δ | | 0 | 0.0981 | 0.1411 | Δ | | 0 | 0.1501 | Δ | | 0.1590 | 0.1906 | 0.2864 |
| | | | +100% | +100% | | | | +100% | | | | +16.58% | +44.48 |

Table 3 lists the O-Si-O, O-Al-O and O-Mg-O bond angles for the bulk and the cuts *1d* and *2d*. Again, two statistical indices are adopted to evaluate the effect of geometry optimization: the average O-Cation-O bond angle per polyhedron, <O-Cation-O> [°], and the difference between the maximum and the minimum bond angles per polyhedron, Δ [°].

The average values computed for the O-Si-O, O-Al-O and O-Mg-O bulk angles are 102.951°, 108.000° and 100.928°, respectively. The most significant O-Si-O, O-Al-O and O-Mg-O variations from the bulk values (+5.52, +0.66 and +2.77%, respectively) after relaxation are observed in the *cut2d* case. The maximum percentage differences between the Δ values in a cut and in the bulk are registered in the *cut2d* as well: they equal -26.79, +85.43 and -94.10% for the O-Mg-O, O-Si-O and O-Al-O bond angles, respectively.

**Table 3. Optimized O-Si-O, O-Al-O and O-Mg-O bond angles [°] of pyrope and of its (100) surface according to the two lowest energy terminations at 0 K, each for the two kinds of cut. Surface data are reported for the symmetry independent polyhedra included in the reconstruction slice. <O-Cation-O> [°] is the average bond angle per polyhedron; Δ [Å] is the difference between the maximum and minimum O-Cation-O angular measures. The relative % difference of <O-Cation-O> and Δ with respect to the bulk, and the multiplicity m of the bond angles in the bulk are reported.**

| angle | m | bulk | (100) *cut1* | (100) *cut2* | angle | m | bulk | (100) *cut2* | angle | m | bulk | (100) *cut1* | (100) *cut2* |
|---|---|---|---|---|---|---|---|---|---|---|---|---|---|
| O-Si-O | 2 | 99.464 | 99.047 | 93.095 | O-Al-O | 6 | 88.133 | 84.493 | O-Mg-O | 2 | 68.823 | 75.041 | 74.061 |
| | 4 | 104.695 | 99.047 | 100.047 | | 6 | 91.867 | 98.562 | | 4 | 70.541 | 81.867 | 75.022 |
| | | | 101.816 | 102.984 | | 3 | 180.000 | 101.460 | | 2 | 72.739 | 81.867 | 90.768 |
| | | | 109.052 | 105.866 | | | | 106.777 | | 4 | 73.301 | 98.767 | 106.994 |
| | | | 109.052 | 122.840 | | | | 129.193 | | 4 | 93.233 | 98.767 | 126.920 |
| | | | 134.897 | 128.988 | | | | 131.822 | | 2 | 109.628 | 179.210 | 149.057 |
| | | | | | | | | | | 2 | 114.854 | | |
| | | | | | | | | | | 4 | 124.338 | | |
| | | | | | | | | | | 2 | 160.211 | | |
| | | | | | | | | | | 2 | 163.908 | | |
| <O-Si-O> | | 102.951 | 108.819 | 108.970 | <O-Al-O> | | 108.000 | 108.718 | <O-Mg-O> | | 100.928 | 102.587 | 103.804 |
| | | | +5.39% | +5.52% | | | | +0.66% | | | | +1.62% | +2.77% |
| Δ | | 5.231 | 35.850 | 35.893 | Δ | | 91.867 | 47.329 | Δ | | 95.085 | 104.169 | 74.996 |
| | | | +85.41% | +85.43% | | | | -94.10% | | | | +8.72% | -26.79% |

## 5. Conclusions

In this paper, we present a work methodology to find all the possible surface configurations of a crystal face obtained by cutting the bulk structure along the crystallographic plane of interest. We have applied our strategy to individuate the surface configurations of the (100), (110) and (112) faces of pyrope. Finally, in order to individuate the most stable surface termination, we have performed an accurate *ab initio* study of the structures and surface energies at 0 K of the (100) configurations, by using for the first time, at the best of our knowledge, the hybrid Hartree-Fock/Density Functional B3LYP Hamiltonian and a localized all-electron Gaussian-type basis set.

We can summarize our results and considerations in the following points:

(i) Twelve initial surface configurations were determined for the (100) face (*cut1a-d* and *cut2a-h*). These configurations were used as guess input geometries by the CRYSTAL09 program for performing *ab initio* calculations and determining in this way the equilibrium structure and surface energy of the most stable surface termination of the (100) face. After the minimization procedure, the twelve initial configurations converged to six, becoming equal two by two: an optimized structure associated to the absolute minimum of the potential energy landscape and five optimized structures corresponding instead to local minima. The lowest surface energy we calculated (1.712-1.720 $J/m^2$) is associated to the *cut1a* and *1d* initial configurations.

(ii) For the (110) and (112) faces the number of initial surface configurations to take into account is considerably higher: 112 and 336, respectively. This prevents the possibility to perform *ab initio* calculations for evaluating the most stable surface termination. The employment of force fields could be a valid alternative to explore all of the identified configurations. Obviously, this implies the use of reliable empirical potentials to describe the interatomic interactions, as for example those implemented into the force field developed by Bosenick et al.[49] for studying the bulk of pyrope and grossular. Anyway, this is out of the scope of the present work, which has as main goal the description of a procedure for determining all of the possible surface configurations of a crystal face.

(iii) An interesting and completely different approach for determining the surface configurations is that developed by the Oganov's research group.[50] They designed an evolutionary algorithm implemented in the USPEX package[51,52] to automatically explore stable and low-energy metastable configurations with variable surface atoms and variable surface unit cells through the whole chemical potential range. By using their strategy, it is not necessary to perform a detailed analysis of the bulk structure as in our method. Indeed, the evolutionary strategy performs an automatic exploration of the energy landscape of surfaces by only specifying an initial surface structure and the chemistry of the system as input. Therefore, in order to

validate our procedure and findings, the use of evolutionary algorithms for the (100), (110) and (112) faces of pyrope should be strongly recommended. Moreover, pyrope could be a stimulating case of study for testing the ability of the evolutionary algorithms into determination of the stable surface configurations on structurally and chemically complex phases.

(iv) It is fundamental to point out that we performed the *ab initio* calculations by only considering the minimum surface cell that allows to perform the reconstruction to obtain a stoichiometric slab. Variable surface cells (i.e.: (100) 2x2, (100) 2x1) should be also considered, in order to increase the degree of freedom of the structure and obtain in this way the configuration with the lowest surface energy. Unfortunately, this requires a heavy computational effort and, at the time being, our calculus resources do not allow a similar in-depth analysis.

(v) Finally, when the stability of a surface is studied, the effect of the temperature must also be taken into account. We have only considered the surface energy at T = 0 K, but it is important to know how this quantity changes with temperature (T > 0 K) by taking into account the entropic contribution due to the vibrational motion of atoms in the bulk crystal and at its surface (vibrational entropy). The effect of the temperature on the surface energy values is not negligible, as recently demonstrated for NaCl and LiF,[46,48,53] for which the value of the surface energy decreases by ~10-15% by increasing the temperature from T = 0 to T = 300 K. Despite that, we believe that for the different (100) surface configurations the decrease of the surface energy due to the temperature is not so different to strongly affect our findings at 0K.

**Supporting Information Available.** Drawings of the unrelaxed and relaxed (100) surface configurations of pyrope ($Mg_3Al_2Si_3O_{12}$): cut1a (Figure S1), cut1b (Figure S2), cut1c (Figure S3), cut2a (Figure S4), cut2b (Figure S5), cut2c (Figure S6), cut2e (Figure S7), cut2f (Figure S8), cut2g (Figure S9) and cut2h (Figure S10). This material is available free of charge via the Internet at http://pubs.acs.org.

**Acknowledgements**

The study was financially supported by ERC 7th Framework Programme "Ideas" Specific Programme, project INDIMEDEA to FN (grant agreement n° 307322). Thanks are due to two anonymous reviewers for their careful reading of the manuscript and their fundamental observations on our work.

**References**


(1) Zhang, L.; Ahsbahs, H.; Kutoglu A. *Physics and Chemistry of Minerals* **1998**, *25*, 301-307.

(2) Deer, W.A.; Howie, R.A.; Zussman, J. *Rock-Forming Minerals*. Volume 1A. Orthosilicates. Longmans, 2nd edition, pp.919.

(3) Nestola, F.; Merli, M.; Nimis, P.; Parisatto, M.; Kopylova, M.; De Stefano, A.; Longo, M.; Ziberna, L.; Manghnani, M. *European Journal of Mineralogy* **2012**, *24*, 599.

(4) Stachel, T.; Harris, J.W. *Ore Geol. Rev.* **2008**, *34*, 5.

(5) Meyer, H.O.A. In: *Mantle Xenoliths*; Nixon, P.H., Ed.; John Wiley & Sons: Chichester, 1987; p.844.

(6) Taylor, L.A.; Anand, M.; Promprated, P. *Proceedings of the 8th International Kimberlite Conference* **2003**, *1*, 1-5.

(7) Meyer, H.O.A. *American Mineralogist* **1985**, *70*, 344.

(8) Harris, J.W. *Ind. Diam. Rev.* **1968**, *28*, 402.

(9) Pearson, D.G.; Shirey, S.B. In: *Application of Radiogenic Isotopes to Ore Deposit Research and Exploration.* Reviews in Economic Geology; Lambert D.D., Ruiz, J., Eds.; Society of Economic Geologists, Littleton CO: Denver, 1999, p.199.

(10) Sobolev, V.S.; Sobolev, N.V.; Lavrent'ev, Y.G. *Dokl. Akad. Nauk. SSR* **1972**, *207*, 164-167.

(11) Harris, J.W.; Gurney, J.J. In: *The properties of diamond*; Field, J.E., Ed.; Academic Press: London, 1979, p. 674.

(12) Mitchell, R.S.; Giardini, A.A. *American Mineralogist* **1953**, *38*, 136.

(13) Futergendler, S.I, Frank-Kamenetsky, V.A. *Zapiski Vsesoyuznogo Mineralogicheskogo Obshestva* **1961**, *90*, 230.

(14) Orlov, J.L. *The mineralogy of diamond*; Wiley: New York, 1977.

(15) Sobolev, N.V. *Deep-seated inclusions in kimberlites and the problem of the composition of theupper mantle*; American Geophysical Union: Washington, DC, 1977.

(16) Leeder, O.; Thomas, R.; Klemm, W. *Einschlusse in Mineralien*; VEB Deutscher Verlag fur Grunstoffen industrie: Leipzig, 1987.

(17) Bulanova, G.P. *J. Geochem. Explor.* **1995**, *53*, 1.

(18) Boutz, M.M.R.; Woensdregt C.F. *Journal of Crystal Growth* **1993**, *134*, 325-336.

(19) Bennema, P.; Giess, E.A.; Weidenborner, J.E. *Journal of Crystal Growth* **1983**, *62*, 41-60.

(20) Pabst, A. *American Mineralogist* **1942**, *28*, 233.

(21) Kretz, A. *The Canadian Mineralogist* **2010**, *48*, 537-548.

(22) Hwang, S.L.; Shen, P.; Chu, H.T.; Yui, T.F.; Iizuka Y. *J. metamorphic Geol.*, **2013**, *31*, 113-130.

(23) Van Haren, J.L.M.; Woensdregt, C.F. *Journal of Crystal Growth* **2001**, *226*, 107-110.

(24) Hartman, P.; Perdok, W.G. *Acta Crystallogr.* **1955**, *8*, 49-52.

(25) Hartman, P.; Perdok, W.G. *Acta Crystallogr.* **1955**, *8*, 521-525.

(26) Hartman, P.; Perdok, W.G. *Acta Crystallogr.* **1955**, *8*, 525-529.

(27) Becke, A.D. *J. Chem. Phys.* **1993**, *98*, 5648.

(28) Lee, C.; Yang, W.; Parr, R.G. *Phys. Rev. B* **1998**, *37*, 785.

(29) Stephens, P.J.; Devlin, F.J.; Chabalowski, C.F.; Frisch, M.J. *J. Phys. Chem.* **1994**, *98*, 11623.

(30) De La Pierre, M.; Bruno, M.; Manfredotti, C.; Nestola, F.; Prencipe, M.; Manfredotti, C. *Molecular Physics* **2013**, doi:10.1080/00268976.2013.829250.

(31) Bruno, M.; Massaro, F.R.; Prencipe, M.; Demichelis, R.; De La Pierre, M.; Nestola, F. **2014**. Ab initio calculations of the main crystal surfaces of forsterite (M2SiO4): a preliminary study to understand the nature of geochemical processes at the olivine interface. *Journal of Physical Chemistry C*, accepted.
(32) Dovesi, R.; Orlando, R.; Civalleri, B.; Roetti, C.; Saunders, V.R.; Zicovich-Wilson, C.M. *Z. Kristallogr* **2005**, *220*, 571.
(33) Dovesi, R. *et al.*, *CRYSTAL09 User's Manual*; University of Torino: Torino, Italy, 2009.
(34) Pisani, C.; Dovesi, R.; Roetti, C. *Hartree-Fockab-initio treatment of crystalline systems*, Lecture Notes in Chemistry; Springer: Berlin, Heidelberg, New York, 1988.
(35) Dovesi, R.; Civalleri, B.; Orlando, R.; Roetti, C.; Saunders, V.R. In: Reviews in Computational Chemistry; Lipkowitz, B.K.; Larter, R.; Cundari, T.R., Eds.; John Wiley & Sons, Inc.: New York, 2005, vol.1, p.443.
(36) Dovesi, R.; De La Pierre, M.; Ferrari A.M.; Pascale, F.; Maschio, L.; Zicovich-Wilson, C.M. *American Mineralogist* **2011**, *96*, 1787-1798.
(37) Noel, Y.; Catti, M.; D'Arco, P.; Dovesi, R. *Phys. Chem. Min.* **2006,** *33*, 383.
(38) Demichelis, R.; Civalleri, B.; Ferrabone, M.; Dovesi, R. *Int. J. Quantum Chem.* **2010**, *110*, 406.
(39) Becke, A.D. *Phys. Rev. A* **1998**, *38*, 3098.
(40) Monkhrost, H.J.; Pack, J.D. *Phys. Rev. B* **1976**, *8*, 5188.
(41) Civalleri, B.; D'Arco, Ph.; Orlando, R.; Saunders, V.R.; Dovesi, R. *Chem. Phys. Lett.* **2001**, *348*, 131.
(42) Doll, K. *Comp. Phys. Commun.* **2001**, *137*, 74.
(43) Doll, K.; Saunders, V.R.; Harrison, N.M. *Int. J. Quantum. Chem.* **2001**, *82*, 1.
(44) Bruno, M. *Crystal Research & Technology* **2013**, *48*, 811-818.
(45) Bruno, M.; Massaro, F.R.; Prencipe, M.; Aquilano, D. *CrystEngComm* **2010**, *12*, 3626-3633.
(46) Bruno, M.; Aquilano, D.; Prencipe, M. *Crystal Growth & Design* **2009**, *9*, 1912-1916.
(47) Bruno, M.; Massaro, F.R.; Prencipe, M. *Surface Science* **2008**, *602*, 2774-2782.
(48) Bruno, M.; Aquilano, D.; Pastero, L.; Prencipe, M. *Crystal Growth & Design* **2008**, *8*, 2163-2170.
(49) Bosenick, A.; Dove, M.T.; Geiger, C.A. *Phys Chem Minerals* **2000**, *27*, 398-418.
(50) Zhu, Q.; Li, L.; Oganov, A.R.; Allen, P.B. *Physical Review B* **2013**, *87*, 195317.
(51) Glass, C.W.; Oganov, A.R.; Hansen, N. *Comp. Phys. Comm.* **2006**, *175*, 713-720
(52) Lyakhov, A.O.; Oganov, A.R.; Stokes, H.T.; Zhu, Q. *Comp. Phys. Comm.* **2013**, *184*, 1172-1182.
(53) Rubbo, M.; Bruno, M.; Prencipe, M. *Crystal Growth & Design* **2009**, *9*, 404−408.

**For Table of Contents Use Only**

# Analysis of the configurations of a crystal surface. Pyrope ($Mg_3Al_2Si_3O_{12}$) as a case of study.

*Massaro F.R.,*[1] *Bruno M.,*[2] *Nestola F.*[1]

[1] Dipartimento di Geoscienze, Università degli Studi di Padova, Via Gradenigo 6, I-35131.

[2] Dipartimento di Scienze della Terra, Università degli Studi di Torino, Via Valperga Caluso 35, I-10125.

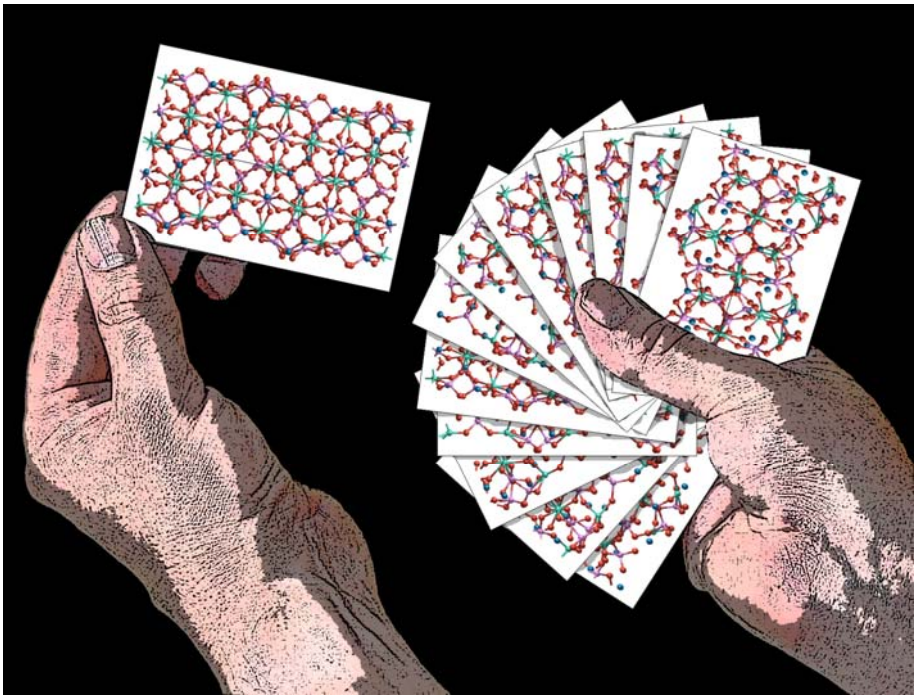

**Synopsis**

A work methodology to determine all the possible surface configurations of a *hkl* crystal face, is presented. This strategy was applied to individuate the surface configurations of the {100}, {110} and {112} forms of pyrope, as a case of study. In order to identify the most stable surface termination, we have performed an *ab initio* study at 0 K of the pyrope {100} configurations, by using the hybrid Hartree-Fock/Density Functional B3LYP Hamiltonian and a localized all-electron Gaussian-type basis set.